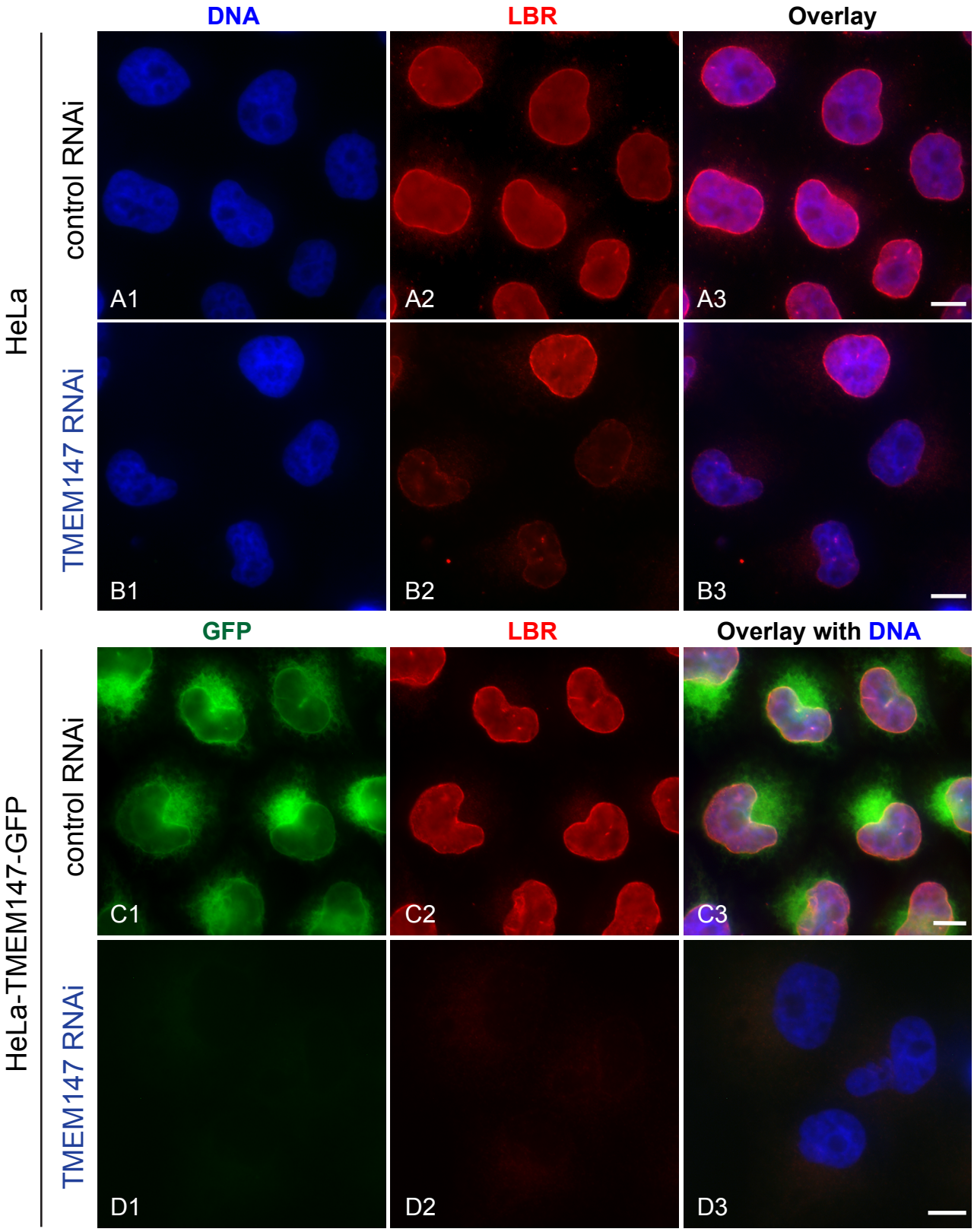

SUPPLEMENTARY FIGURE 1

FIGURE S1

Effect of *TMEM147* silencing on LBR

(A, B series) Representative examples of loss of immunofluorescence for LBR (red) during silencing of *TMEM147* in HeLa cells (compare control silencing in panels A with *TMEM147* silencing in panels B). Nuclei were counterstained for DNA (blue), and overlay images display blue and red fluorescence concurrently.

(C, D series) Equivalent analysis as for A+B, but using the stably transfected TMEM147-GFP cell line, where GFP fluorescence serves as a marker for the expression of TMEM147-GFP (green). Again, LBR expression (red) is extremely reduced upon *TMEM147* silencing. Overlay images display GFP, LBR labeling together with blue Hoechst counterstaining for nuclei. Scale bars 10 μm.

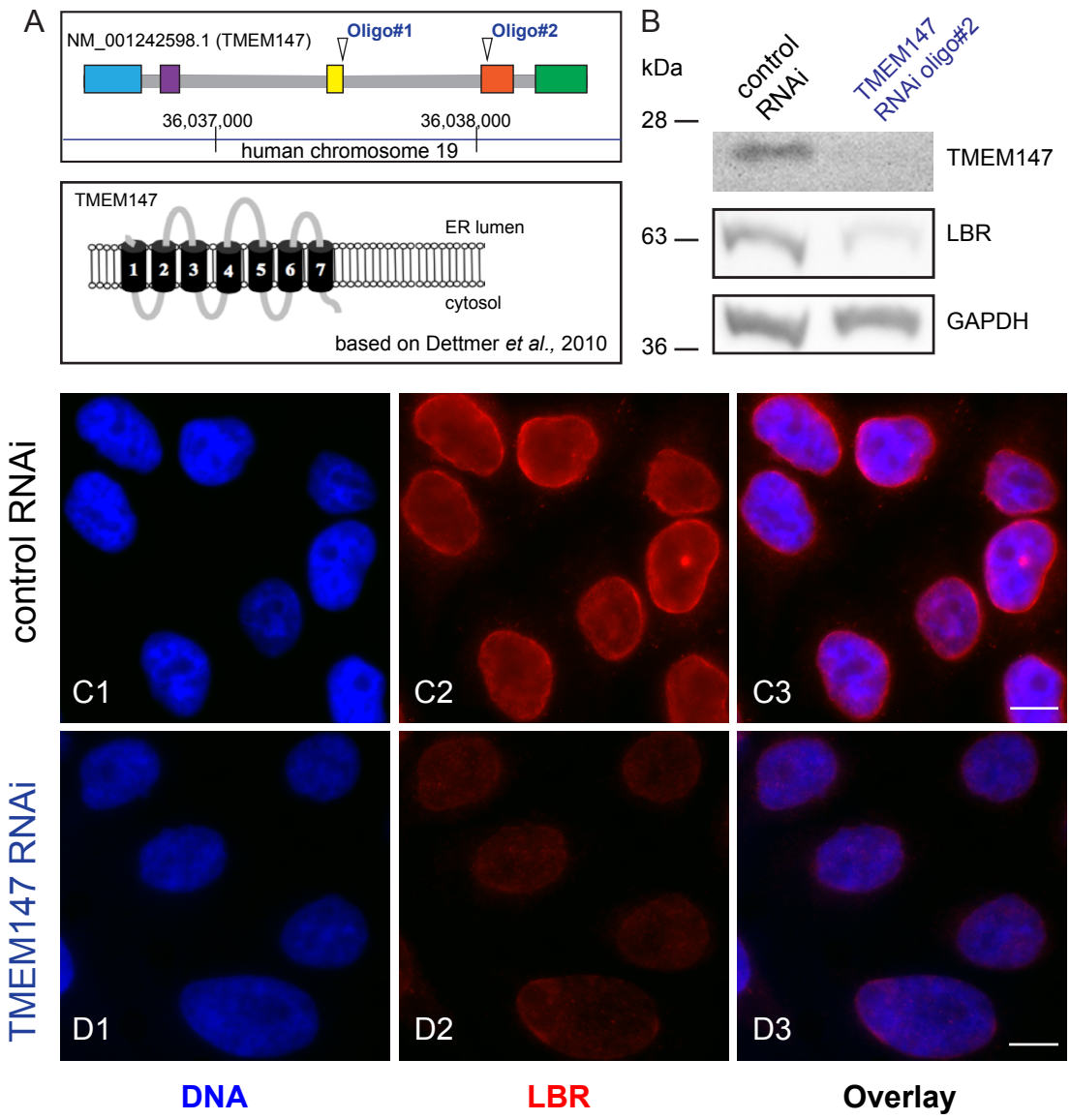

SUPPLEMENTARY FIGURE 2

FIGURE S2

Confirmation of effect of *TMEM147* silencing on LBR using an alternative siRNA silencing oligo

(A) (Top panel) Sketch of the multi-exon mRNA organization of human *TMEM147*, highlighting the targeting positions of the siRNA oligonucleotide 1 (oligo#1), used for silencing experiments in Figs. 2, 3, 4, 6 and 7, and siRNA oligonucleotide 2 (oligo#2) used in the current figure for confirmation of the specificity of the silencing phenotypes and in particular the effect on LBR.

(Bottom panel) Sketch of the model, based on Dettmer et al., 2010, of the multidomain topology of TMEM147 in the ER membranes.

(B) Similar to oligo#1 (Fig. 1 and 2), siRNA-silencing with oligo#2, is efficient in knocking down *TMEM147* (top panel), as assessed by WB analysis, and in drastically reducing LBR protein levels (middle panel). GAPDH serves as loading control.

(C, D series) Immunofluorescence analysis of HeLa cells silenced with oligo#2 (panels D1-D3), replicates significant loss of LBR labeling (red in D2), as compared with control-silenced cells (panels C1-C3, red in C2). Nuclei are labeled by Hoechst (blue) and overlay images combine LBR and DNA signals. Scale bars 10 μm.

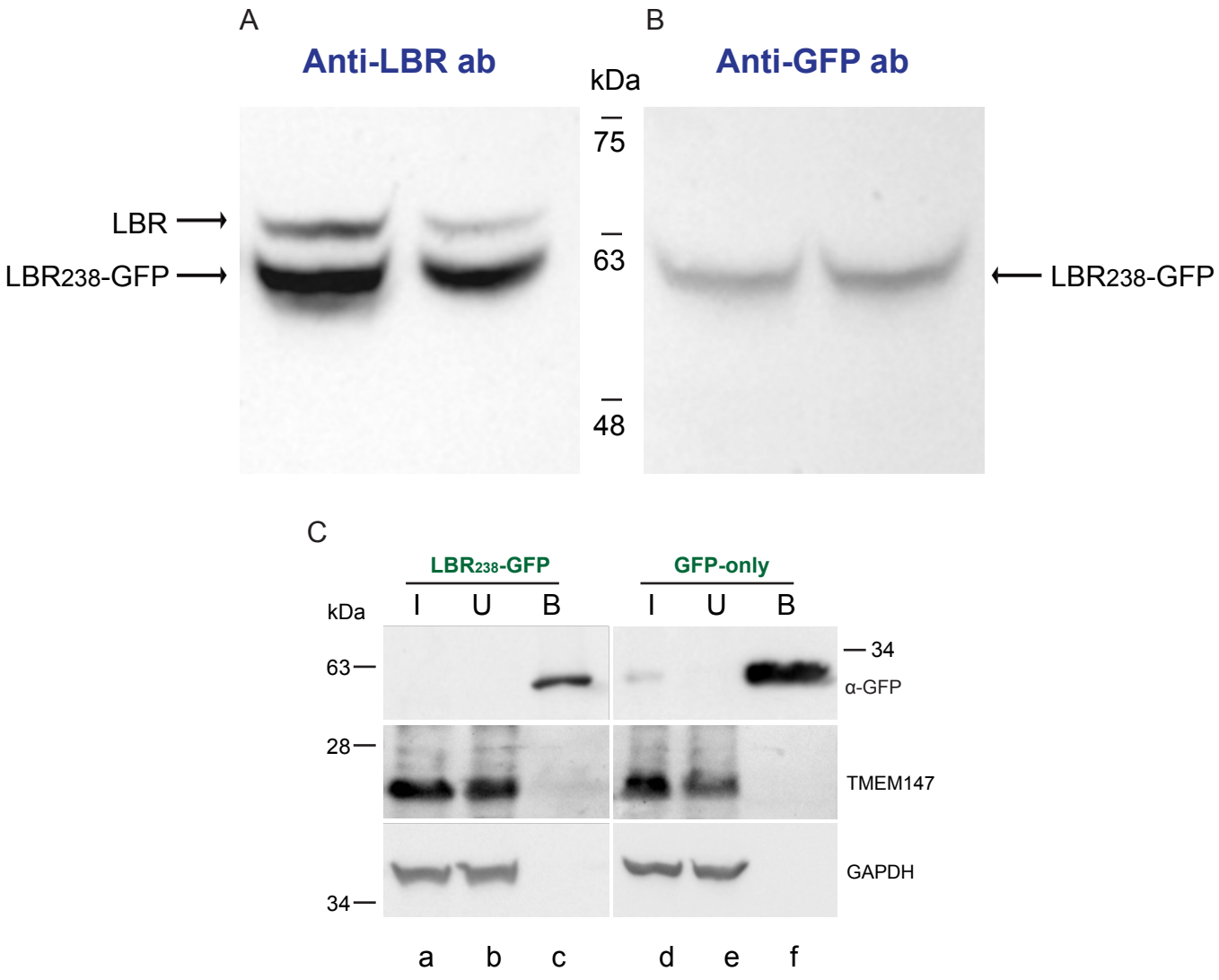

SUPPLEMENTARY FIGURE 3

FIGURE S3

Expression and detection of LBR238-GFP in the stable LBR238-GFP HeLa cell line

(A) Application of anti-LBR antibody in a total protein extract from the stable LBR238-GFP HeLa cell line results in the detection of an upper band of molecular mass close to 63kDa, that corresponds to endogenous full-length LBR, and a faster-migrating lower band, corresponding to LBR238-GFP.

(B) Use of anti-GFP antibody with the same samples appropriately only detects the lower band with the GFP-tagged protein.

(C) Test and negative control experiments, in parallel to the analysis shown in Fig.6 B5. Samples shown here were from HeLa cells transfected with N-terminal construct LBR238-GFP or with GFP-only construct. Top panels confirm binding of GFP-tagged versions of LBR or GFP-only in the bound fractions as bait; middle panels indicate absence of co-selection of native TMEM147 in the bound fractions; bottom panel displays GAPDH immunoreactivity as loading control. Abbreviations: (I) input, (U)"unbound, and (B) bound fractions.

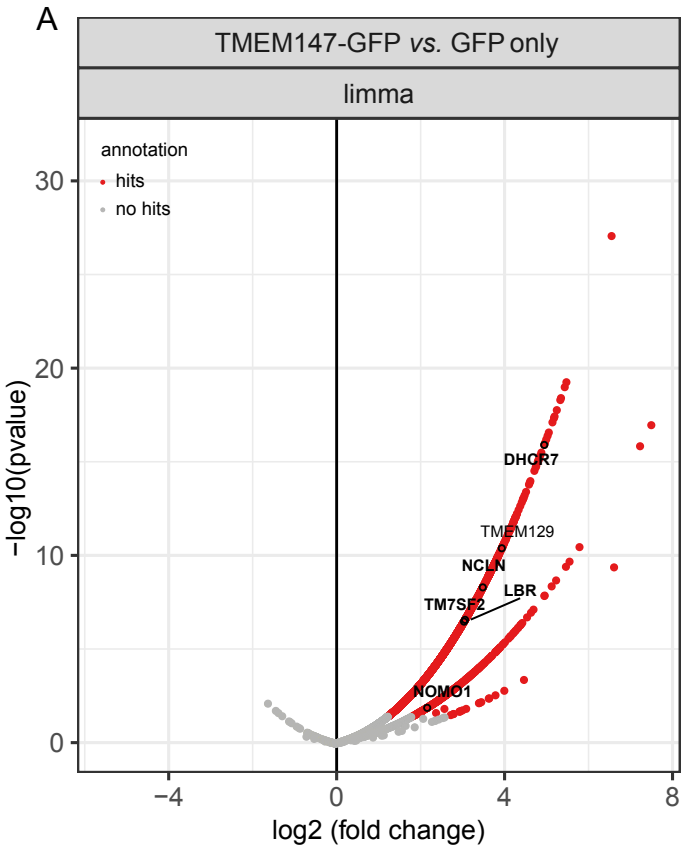

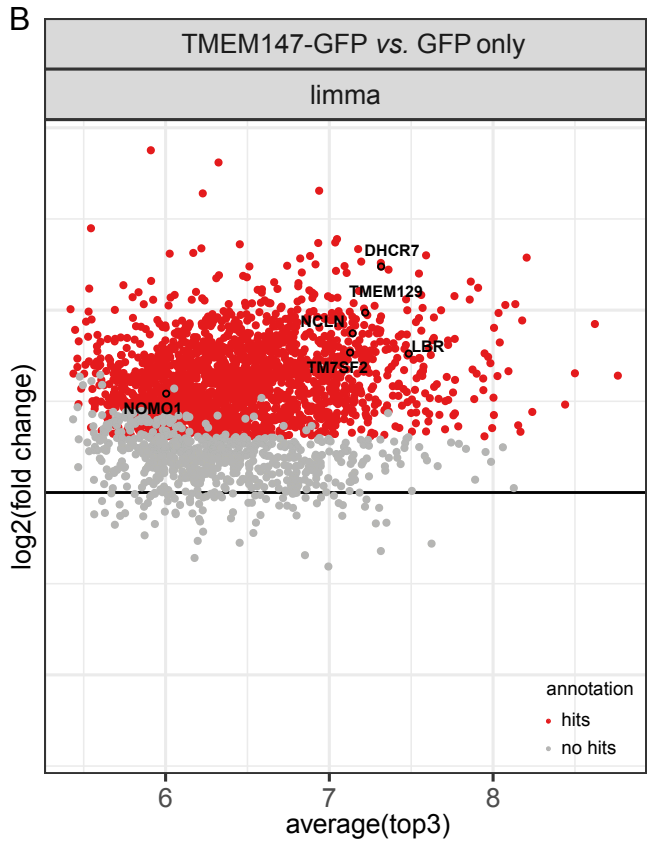

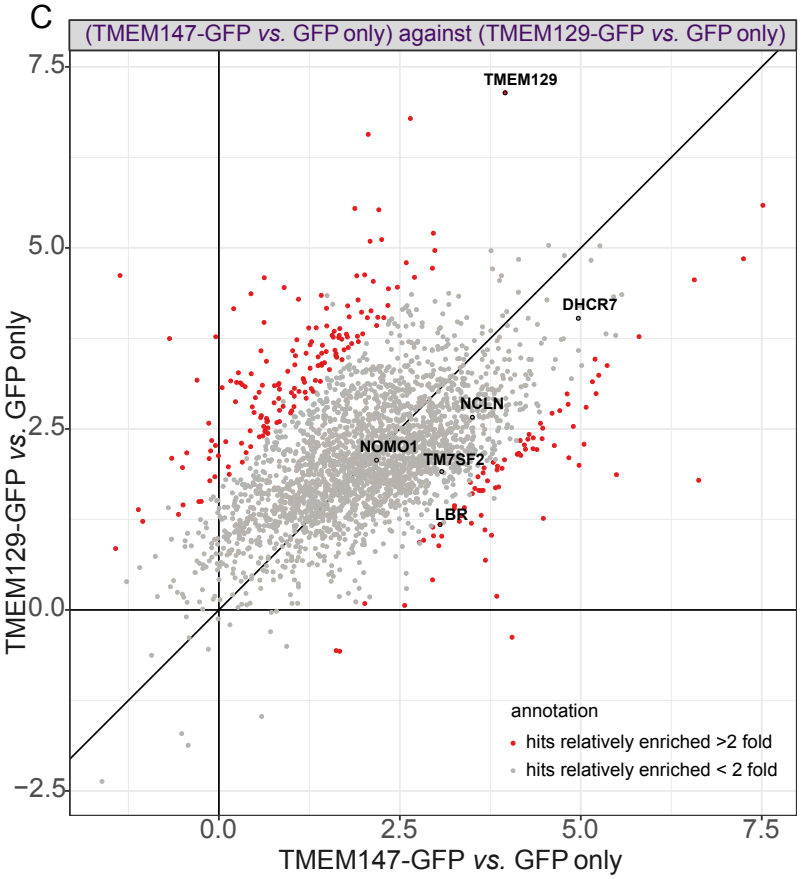

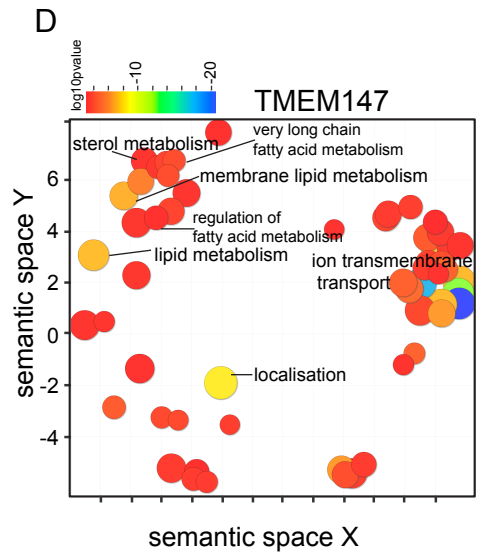

term_ID	description	frequency	log10 p-value	uniqueness
GO:0006629	lipid metabolic process	3.522%	-7.3809	0.850
GO:0006643	membrane lipid metabolic process	0.382%	-7.1018	0.734
GO:0044255	cellular lipid metabolic process	2.704%	-5.6038	0.702
GO:0006633	fatty acid biosynthetic process	0.617%	-4.2503	0.680
GO:0006650	glycerophospholipid metabolic process	0.543%	-3.0996	0.687
GO:0046486	glycerolipid metabolic process	0.593%	-3.3316	0.726
GO:0008654	phospholipid biosynthetic process	0.889%	-4.0958	0.662
GO:0008610	lipid biosynthetic process	2.123%	-4.5686	0.706
GO:0071702	organic substance transport	4.980%	-7.3363	0.704
GO:0042761	very long-chain fatty acid biosynthetic process	0.009%	-4.1361	0.754
GO:0016125	sterol metabolic process	0.106%	-3.2351	0.757
GO:0008203	cholesterol metabolic process	0.028%	-3.1397	0.760
GO:0046949	fatty-acyl-CoA biosynthetic process	0.003%	-3.2248	0.906
GO:0055085	transmembrane transport	8.916%	-12.7375	0.685
GO:0000038	very long-chain fatty acid metabolic process	0.018%	-3.3635	0.766
GO:0006869	lipid transport	0.270%	-4.6253	0.647
GO:0030497	fatty acid elongation	0.010%	-3.8013	0.753
GO:0019217	regulation of fatty acid metabolic process	0.021%	-3.1325	0.705
GO:0006665	sphingolipid metabolic process	0.093%	-5.9914	0.742
GO:0046467	membrane lipid biosynthetic process	0.317%	-4.9101	0.705
GO:0006684	sphingomyelin metabolic process	0.007%	-4.1096	0.747
GO:0030148	sphingolipid biosynthetic process	0.032%	-3.6055	0.741

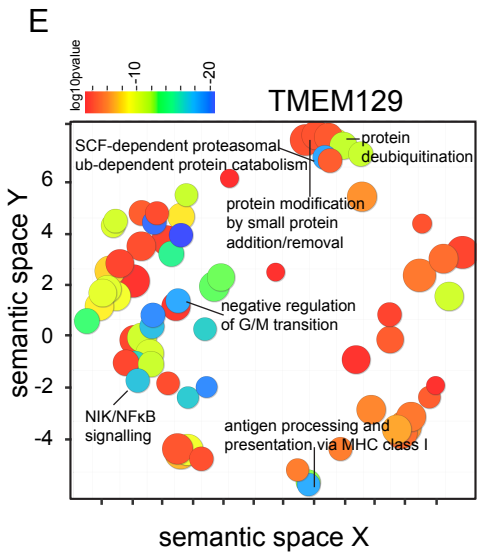

term_ID	description	frequency	log10 p-value	uniqueness
GO:0002376	immune system process	0.600%	-7.3757	0.989
GO:0031146	SCF-dep proteasomal ub-dep protein catabolic process	0.022%	-11.1824	0.812
GO:0030163	protein catabolic process	0.997%	-6.5003	0.808
GO:0043161	proteasome-mediated ub-dep protein catabolic process	0.226%	-6.2503	0.780
GO:0044265	cellular macromolecule catabolic process	1.268%	-4.6216	0.802
GO:0019941	modification-dependent protein catabolic process	0.612%	-6.8729	0.767
GO:0043632	modification-dependent macromolecule catabolic process	0.627%	-6.1180	0.807
GO:0051603	proteolysis involved in cellular protein catabolic process	0.759%	-7.8153	0.764
GO:0006511	ubiquitin-dependent protein catabolic process	0.584%	-5.9469	0.767
GO:0031145	anaphase-promoting complex-dep catabolic process	0.021%	-10.4908	0.812
GO:0010498	proteasomal protein catabolic process	0.267%	-5.9393	0.782
GO:0010972	negative regulation of G2/M transition of mitotic cell cycle	0.027%	-11.1255	0.679
GO:0038061	NIK/NF-kappaB signaling	0.018%	-10.6308	0.691
GO:0019221	cytokine-mediated signaling pathway	0.093%	-10.2741	0.574
GO:0016579	protein deubiquitination	0.195%	-7.7033	0.833
GO:0016567	protein ubiquitination	0.523%	-5.7212	0.835
GO:0070646	protein modification by small protein removal	0.219%	-6.9547	0.832
GO:0000209	protein polyubiquitination	0.066%	-7.5452	0.858
GO:0032446	protein modification by small protein conjugation	0.607%	-4.3979	0.834
GO:0002474	antigen processing+presentation via MHC class I	0.010%	-11.0585	0.717
GO:0070647	protein modification by small protein conjugation/removal	0.821%	-3.7144	0.847

SUPPLEMENTARY FIGURE 4

FIGURE S4

TMEM147 interacts with DHCR7

Bound proteins from IP experiments using as baits TMEM147-GFP, TMEM129-GFP (for comparison) and GFP-only (negative control) were processed and extracted peptides subjected to liquid chromatography coupled with tandem mass spectrometry for protein identification.

(A) Volcano plot with identified hit proteins for TMEM147 (using GFP-only as negative control), in which some proteins of interest (POIs) are indicated (DHCR7, LBR, TM7SF2 and, known TMEM147 interactors, NOMA and Nicalin, NCLN).

(B) Corresponding TOP3 plot with the same proteins highlighted.

(C) Comparison of enrichment between the TMEM147 and TMEM129 hits (using in both cases GFP-only as negative control).

(D, E) Gene Ontology (GO) analysis of top biological processes identified from the ranked hits for TMEM147 (D) and TMEM129 (E), using *GOrilla* (Gene Ontology enRIchment anaLysis and visuaLizAtion tool; http://cbl-gorilla.cs.technion.ac.il/) and REVIGO (REduce and VIsualize Gene Ontology; http://revigo.irb.hr/). "*Lipid metabolism*", "*membrane lipid biosynthesis*" and "*sterol metabolism*" were among the top GO terms (statistical significance, frequency and uniqueness) associated with TMEM147, consistent with our findings. For TMEM129 (an ERAD E3 ubiquitin ligase, essential for virus-induced degradation of MCH-I; van den Boomen et al., 2014 van de Weijer et al., 2014), top GO terms included "*SCF-dependent proteasomal ubiquitin-dependent protein catabolic process*" and "*antigen processing and presentation of peptide antigen via MHC class I*", again consistent with its characterised function. The associated tables display some examples of top GO terms, selected for their relevance.

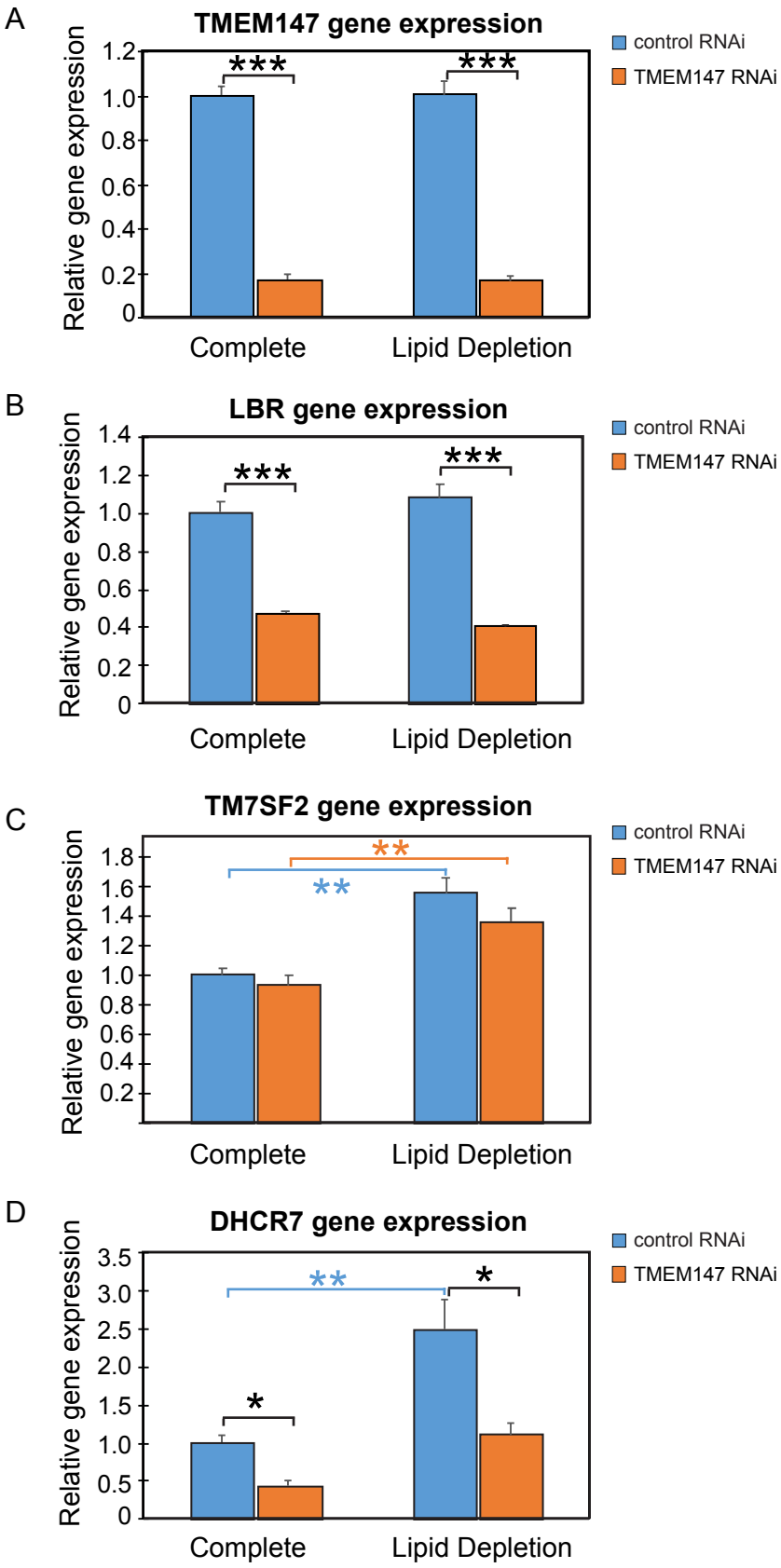

SUPPLEMENTARY FIGURE 5

FIGURE S5

Assessment by RT-qPCR in three independent experiments of *TMEM147, LBR*, *DHCR7* and *TM7SF2* mRNA levels in negative control and *TMEM147*-silenced cells grown in parallel, either in full media (72 h) or in lipid restrictive media (48 h in complete media and serum starved for 24 h). To be directly comparable, values are calculated using the common base method (Ganger et al., 2017) and expressed as a ratio to the normalized mean control value with error bars corresponding to SE of triplicate analysis. The results show that both *TMEM147* and *LBR* are constitutively expressed, irrespective of lipid restriction and their co-ordinate downregulation upon *TMEM147* silencing remains unchanged (A and B). Lipid restriction induces statistically significant and almost identical *TM7SF2* upregulation both in the presence and absence of *TMEM147* (C). *DHCR7* expression is even more markedly induced upon lipid restriction, specifically 2.5-fold in the presence of *TMEM147* (from 1.00±0.10 relative expression in complete medium to 2.49±0.40 upon lipid restriction, p=0.007). The absence of *TMEM147* induces downregulation of *DHCR7*, as also seen in Fig. 7C, both in normal conditions and in lipid restriction, but although the absolute values of *DHCR7* exression are reduced, the 2.5-fold induction ratio of *DHCR7* expression is maintained upon lipid restriction (from 0.44±0.07 in complete medium to 1.11±0.15 upon lipid restriction, p=0.01).

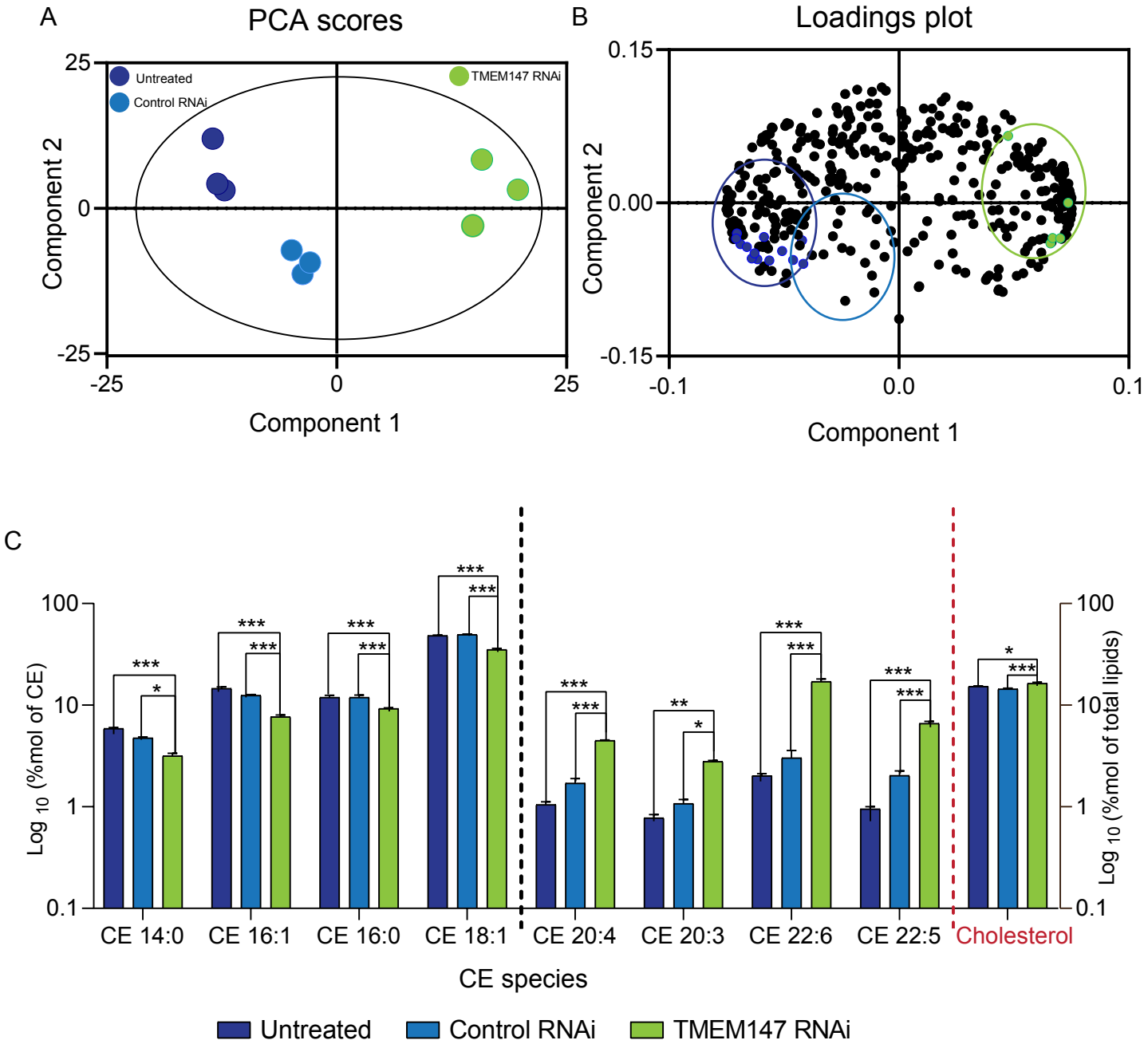

SUPPLEMENTARY FIGURE 6

FIGURE S6

Lipidomic rewiring in TMEM147 silenced HeLa cells.

(A) PCA (principal component analysis) scores plot of the total lipid profiles in untreated, control and" TMEM147 silenced cells. **(B)** PCA loadings plot showing the lipid species influence on the separation" between untreated, control and *TMEM147* silenced cells. **(C)** Most important CE species and" cholesterol in untreated, control- and *TMEM147*-silenced cells. Data are presented as mean±SEM and" analysed by 2-way ANOVA with post hoc Tukey's multiple-comparisons test; *$p \leq 0.05$, ** $p \leq 0.01$," *** $p \leq 0.001$ n = 3/group.

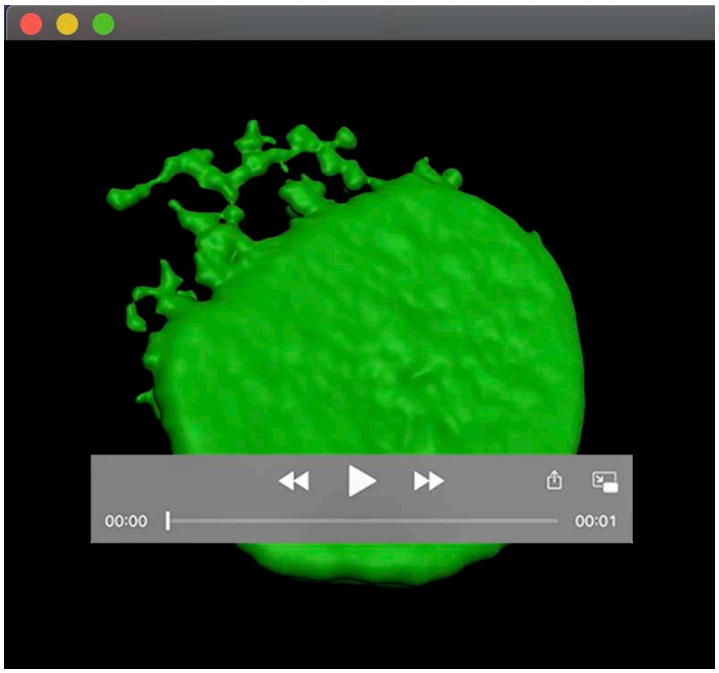

Movie 1

Animation of 3D rendering of one of the silenced cells in Fig. 6D, to illustrate enhanced LBR mislocalization at the ER upon *TMEM147* silencing.

TABLE S1

Percentages of cells exhibiting LBR labeling at the NE only or partitioning between the NE+ER.

	No. cells with NE-localized LBR (% of population)	No. cells with ER-localized LBR (% of population)	No. cells with unclear localization	Total number of cells
Control RNAi	47 (**85.5%**)	6 (**10.9%**)	2	55
TMEM147 RNAi	15 (**31.3%**)	31 (**64.6%**)	2	48

TABLE S2

Click here to Download Table S2